

# Constructing a map from the electron density to the exchange–correlation potential

Julius B. Lucks,<sup>ab</sup> Aron J. Cohen<sup>\*a</sup> and Nicholas C. Handy<sup>a</sup>

<sup>a</sup> Department of Chemistry, University of Cambridge, Cambridge, UK CB2 1EW.

E-mail: [ajc54@cam.ac.uk](mailto:ajc54@cam.ac.uk)

<sup>b</sup> Department of Chemistry and Chemical Biology, Harvard University, Cambridge MA 02138, USA

Received 17th June 2002, Accepted 23rd July 2002

First published as an Advance Article on the web 5th September 2002

Near-exact exchange–correlation potentials calculated with the procedure of Zhao, Morrison and Parr (ZMP) for 35 systems are combined in a histogram average to construct an exchange–correlation potential. The histogramming scheme makes use of a self-adjusting Cartesian grid (SACG), whereby the bin size is adjusted based on the number of data points in a region. The two-dimensional SACG approach is first tested against an analytic exchange–correlation potential of two-variables and shown to reproduce it to the required accuracy. The SACG approach is then applied to the ZMP data, and Kohn–Sham eigenvalues and densities are compared. Further extensions are discussed.

## 1 Introduction

Density functional theory (DFT) has made a large contribution to computational chemistry.<sup>1,2</sup> In particular, the developments of Kohn and Sham<sup>3</sup> have provided a practical approach to DFT of atoms and molecules and have created a framework within which DFT can be systematically improved, through successive approximations to the unknown exchange–correlation energy,  $E_{xc}$ . However, only the functional derivative of  $E_{xc}$ , the exchange–correlation potential,  $v_{xc}$ , is required to solve the Kohn–Sham equations for the Kohn–Sham orbitals which give the density,  $\rho$ , by construction. The density is the fundamental quantity of DFT since by the first Hohenberg–Kohn theorem<sup>4</sup> it determines *all* properties of a system. We are thus motivated to attack approximations to  $v_{xc}$  directly instead of going through the functional  $E_{xc}$ .

This idea is not new. Some efforts have made use of exact properties of  $v_{xc}$ , such as asymptotic limits<sup>5</sup> and coordinate scaling.<sup>6</sup> Others have proposed functional forms with adjustable parameters determined by fitting to near-exact  $v_{xc}$  data.<sup>7</sup>

Our approach starts with near-exact  $v_{xc}$  data. Zhao, Morrison and Parr (ZMP) have developed a scheme whereby a near-exact density is used to compute  $v_{xc}(\mathbf{r})$  along with density variables such as  $\rho(\mathbf{r})$ ,  $|\nabla\rho(\mathbf{r})|$ ,  $\nabla^2\rho(\mathbf{r})$ ,  $\nabla\rho(\mathbf{r})\cdot\nabla\nabla\rho(\mathbf{r})\cdot\nabla\rho(\mathbf{r})$ , *etc.* on a spatial grid for a system of choice.<sup>8</sup> We use this information from a chosen fit set of systems to construct a map from a set of density variables of choice at a point,  $\mathbf{r}$ , to the exchange–correlation potential at that point,  $v_{xc}(\mathbf{r})$ . Instead of using this data to determine parameters in a proposed analytical map, we construct a histogram representation of the potential, which can subsequently be used in Kohn–Sham calculations. This histogram map can be constructed in any dimensions of choice: this work focuses on the  $(\rho, |\nabla\rho|)$  plane because of the success of generalized-gradient approximations (GGA) to  $E_{xc}$ . The goals of this paper are twofold: 1. to motivate, establish and demonstrate the effectiveness of the numerical histogram mapping scheme, and 2. to apply the histogramming approach to create a map to  $v_{xc}^{ZMP}$ , since  $v_{xc}^{ZMP}$  represents the true exchange–correlation potential for a system.

The ZMP method is discussed in section 2. The two-dimensional histogram method itself is then discussed in section 3, followed by an analysis of how the histogram method performs on an analytic function of only two dimensions in section 4. We end with results on the application to ZMP potentials and conclusions in sections 5 and 6, respectively.

## 2 The Zhao, Morrison, Parr method

The Kohn–Sham orbitals are the set of orbitals,  $\{\phi_i^{KS}\}$ , that minimize the non-interacting kinetic energy,<sup>9</sup>  $T_s$ , given by

$$T_s[\{\phi_i\}] = \sum_i^N \left\langle \phi_i \left| -\frac{1}{2}\nabla^2 \right| \phi_i \right\rangle \quad (1)$$

where  $N$  is the number of occupied orbitals, and give the ground-state density,  $\rho_0$ , by

$$\rho_0 = \sum_i^N |\phi_i^{KS}(\mathbf{r})|^2 \quad (2)$$

One way to solve for these orbitals is to constrain eqn. (2) in the minimization of eqn. (1) with respect to  $\{\phi_i\}$  with the method of Lagrange multipliers, which requires an undetermined multiplier at each point in space,  $\lambda(\mathbf{r})$ . Zhao and Parr<sup>10</sup> recognized that a more efficient way to invoke the constraint is through the non-local expression

$$C[\rho, \rho_0] = \frac{1}{2} \iint \frac{(\rho(\mathbf{r}) - \rho_0(\mathbf{r}))(\rho(\mathbf{r}') - \rho_0(\mathbf{r}'))}{|\mathbf{r} - \mathbf{r}'|} d\mathbf{r}d\mathbf{r}' \quad (3)$$

which only requires a scalar multiplier,  $\lambda$ . Since the energy due to the external potential,  $E_{ext}[\rho]$ , and the Coulomb energy,  $J[\rho]$ , are explicit functionals of the density and do not depend on the individual orbitals, these quantities can be added to  $T_s[\rho]$  and the orbitals at the minimum will not change. Performing the minimization of  $T_s[\rho] + E_{ext}[\rho] + J[\rho]$  with respect to changes in the orbitals with the constraint eqn. (3) and imposing orthonormality

$$\int \phi_i^*(\mathbf{r})\phi_j(\mathbf{r})d\mathbf{r} = \delta_{ij} \quad (4)$$

we obtain the set of canonical equations

$$\left(-\frac{1}{2}\nabla^2 + \lambda v_c^\lambda(\mathbf{r}) + v_{\text{ext}}(\mathbf{r}) + \frac{N-1}{N}v_j^\lambda - \varepsilon_i^\lambda\right)\phi_i^\lambda = 0$$

$$i = 1, 2, \dots \quad (5)$$

where  $v_{\text{ext}}(\mathbf{r})$  is the external potential,  $v_j^\lambda$  is the Coulomb potential

$$v_j^\lambda = \int \frac{\rho^\lambda(\mathbf{r}')}{|\mathbf{r} - \mathbf{r}'|} d\mathbf{r}' \quad (6)$$

$v_c^\lambda(\mathbf{r})$  is the constraint potential

$$v_c^\lambda(\mathbf{r}) = \int \frac{(\rho^\lambda(\mathbf{r}') - \rho_0(\mathbf{r}'))}{|\mathbf{r} - \mathbf{r}'|} d\mathbf{r}' \quad (7)$$

and we have multiplied  $v_j^\lambda$  by the Fermi–Amaldi factor<sup>11</sup> following ZMP.<sup>8</sup> The density  $\rho^\lambda$  is given by

$$\rho^\lambda = \sum_i^N |\phi_i^\lambda|^2 \quad (8)$$

The solution point is reached when  $\rho^\lambda = \rho_0$ , which is achieved in the limit  $\lambda \rightarrow \infty$ .<sup>7</sup> At the solution point, these eqns. (5) minimize  $T_s$  and thus are the Kohn–Sham equations.<sup>8</sup> Noting the form of the Kohn–Sham effective potential<sup>3</sup>

$$v_{\text{eff}}^{\text{KS}}(\mathbf{r}) = v_J(\mathbf{r}) + v_{\text{ext}}(\mathbf{r}) + v_{\text{xc}}(\mathbf{r}) \quad (9)$$

we find

$$v_{\text{xc}}^{\text{ZMP}}(\mathbf{r}) = \lim_{\lambda \rightarrow \infty} \left( \lambda v_c^\lambda(\mathbf{r}) - \frac{1}{N} \int \frac{\rho^\lambda(\mathbf{r}')}{|\mathbf{r} - \mathbf{r}'|} d\mathbf{r}' \right) \quad (10)$$

It is important to view the result eqn. (10) in light of the work of Perdew, Parr, Levy and Balduz (PPLB)<sup>12</sup> and Perdew and Levy<sup>13</sup> who examined DFT for fractional numbers of particles. PPLB noted that as a function of the number of particles, the energy has discontinuous derivatives at integer particle numbers,

$$\left. \frac{\partial E_N}{\partial N} \right|_{N-\delta} = \frac{E_N - E_{N-1}}{N - (N-1)} = E_N - E_{N-1} = -I$$

$$\left. \frac{\partial E_N}{\partial N} \right|_{N+\delta} = \frac{E_{N+1} - E_N}{(N+1) - N} = E_{N+1} - E_N = -A \quad (11)$$

where  $0 < \delta < 1$ . By Janak's theorem,<sup>14</sup> the HOMO eigenvalue thus jumps at the integer

$$\left. \frac{\partial E_N}{\partial n_N} \right|_{N-\delta} = \varepsilon_N|_{N-\delta} = -I$$

$$\left. \frac{\partial E_N}{\partial n_{N+1}} \right|_{N+\delta} = \varepsilon_{N+1}|_{N+\delta} = -A \quad (12)$$

since changes in particle number are achieved through changing the occupation numbers of the Kohn–Sham orbitals,  $n_i$ . The density is continuous with respect to changes in particle number, thus the only element of the Kohn–Sham equations that could achieve this jump is  $v_{\text{xc}}$  and they noted

$$\lim_{\delta \rightarrow 0} v_{\text{xc}}|_{N+\delta} - \lim_{\delta \rightarrow 0} v_{\text{xc}}|_{N-\delta} = C_{\text{sys}} \quad (13)$$

where the constant is system-dependent because of the nature of the discontinuity eqn. (12).

In wave-function based approaches to quantum chemistry, there is an inherent discontinuity in changing particle numbers because the wave function must change number of variables. In DFT however, the density is continuous with respect to changing particle numbers, and we would expect some smooth

transition from  $N - \delta$  to  $N + \delta$  particles to occur. This is indeed the case as shown by Perdew and Levy.<sup>13</sup>

$$v_{\text{xc}}|_N = \frac{1}{2} \left( \lim_{\delta \rightarrow 0} v_{\text{xc}}|_{N-\delta} + \lim_{\delta \rightarrow 0} v_{\text{xc}}|_{N+\delta} \right) \quad (14)$$

The asymptotic form of the density is given by<sup>15</sup>

$$\lim_{r \rightarrow \infty} \rho(\mathbf{r}) = \exp[-2(2I)^{1/2}r] \quad (15)$$

When this is used in the asymptotic limit of the Kohn–Sham equations, we see

$$\lim_{r \rightarrow \infty} v_{\text{xc}}(\mathbf{r}) = I + \varepsilon_{\text{KS}}^{\text{HOMO}} \quad (16)$$

We now find a perspective with which to view the ZMP potential,  $v_{\text{xc}}^{\text{ZMP}}$ . By eqn. (10)  $v_{\text{xc}}^{\text{ZMP}}$  goes to zero in the asymptotic limit, and thus  $\varepsilon_{\text{xc}}^{\text{HOMO}} = -I$  by eqn. (16). According to the PPLB analysis,  $v_{\text{xc}}^{\text{ZMP}}$  corresponds to the negative side of the integer discontinuity (12). Using this in eqns. (13) and (14), we find

$$v_{\text{xc}}|_N = v_{\text{xc}}^{\text{ZMP}} + \frac{C_{\text{sys}}}{2} \quad (17)$$

This has very important implications for this study. If we were only concerned with  $v_{\text{xc}}^{\text{ZMP}}$  for one system at a time, this result would be insignificant since shifting a potential by a constant does not change the orbitals. However, in this study,  $v_{\text{xc}}^{\text{ZMP}}$  from several systems are combined together. If the system-dependent shifts were not included, the data for each system would represent  $v_{\text{xc}} - C_{\text{sys}}/2$  by eqn. (17), and would effectively be scrambled. The constructed potential would have no hope of approximating a true functional derivative. Thus it is vital to include a system-dependent shift for each  $v_{\text{xc}}^{\text{ZMP}}$ .

This analysis has previously been noted by Tozer and Handy<sup>16</sup> in the context of  $E_{\text{xc}}$  development. In their fitting procedure, they included a system-dependent shift, which was determined by minimizing errors in the exchange–correlation potential with respect to  $v_{\text{xc}}^{\text{ZMP}}$  data. We use similar values, calculated in the context of the functional of Hamprecht *et al.*,<sup>17</sup> as the system-dependent shifts, and they are shown in Table 1.

The fit set of molecules used to construct the potential map are shown in Table 1. This study is restricted to closed-shell systems and potentials. For each system in the fit set, accurate *ab initio* electron densities were computed using the Brueckner doubles<sup>18</sup> coupled cluster technique with a TZ2P<sup>19</sup> basis set. These densities were used in the ZMP code developed by Tozer *et al.*<sup>7</sup> As recommended by these authors, the value  $\lambda = 900$  was used to reduce errors caused by using finite basis sets. The ZMP potentials were calculated on a numerical, spatial grid and were used along with values of  $\rho$ ,  $|\nabla\rho|$ ,  $\nabla^2\rho$ ,  $\nabla\rho \cdot \nabla\nabla\rho \cdot \nabla\rho$ , *etc.* on the grid as the input data set for the potential construction method discussed below.

### 3 The self-adjusting Cartesian grid

As mentioned in the introduction, once accurate  $v_{\text{xc}}$  data is available, one approach to construct an exchange–correlation potential would be to fit the data to a proposed function form. When fitting a data set of  $p$  points,  $\mathbf{D}(p)$ , with a function of  $n$  parameters, care must be taken so that  $n$  does not become greater than  $p$  as this causes instability of the fit, and is known as *over-fitting*.<sup>20</sup> In addition, the basis set of fitting functions used to create the proposed function often does not span the space of functions and thus even in the data-set limit, where the set  $\mathbf{D}(p)$  contains all data points necessary to completely determine the original function, the true function whence the set  $\mathbf{D}(p)$  came is not reproduced by the fit.

To alleviate these drawbacks, we examine a grid-based scheme whereby the actual data points  $\mathbf{D}(p)$  are used with

**Table 1** For each system in the fit set: Index denotes the system index used in Figs. 3 and 4;  $n_{\text{occ}}$  is the number of occupied Kohn–Sham orbitals;  $C_{\text{sys}}(E_h)$  from eqn. (17) are taken from the analysis of TH<sup>16</sup> as applied to the functional of Hamprecht *et al.*,<sup>17</sup> where the factor of  $\frac{1}{2}$  is implicit; RMS denotes root mean square errors (eqn. (19)) of occupied Kohn–Sham eigenvalues between analytic LB94 and  $^{\text{LB94}}\text{SACG}(\rho,|\nabla\rho)|_{50}^{0.5}$  and between ZMP and  $^{\text{ZMP-TH}}\text{SACG}(\rho,|\nabla\rho)|_{50}^{0.5}$  potentials. The  $^{\text{ZMP-TH}}\text{SACG}(\rho,|\nabla\rho)|_{50}^{0.5}$  eigenvalues are corrected for the  $C_{\text{sys}}$  shifts

| System  | Index | $n_{\text{occ}}$ | $C_{\text{sys}}$ | RMS    |        | System                        | Index | $n_{\text{occ}}$ | $C_{\text{sys}}$ | RMS    |        |
|---|-------|------------------|------------------|--------|--------|-------------------------------|-------|------------------|------------------|--------|--------|
|   |       |                  |                  | LB94   | ZMP    |                               |       |                  |                  | LB94   | ZMP    |
| Al <sup>+</sup>                                 | 1     | 6                | 0.0839           | 0.0386 | 0.1239 | C <sub>2</sub> H <sub>2</sub> | 2     | 7                | 0.1281           | 0.0095 | 0.0444 |
| C <sub>2</sub> H <sub>4</sub>                   | 3     | 8                | 0.1286           | 0.0098 | 0.0444 | C <sub>2</sub> H <sub>6</sub> | 4     | 9                | 0.1330           | 0.0087 | 0.0434 |
| CH <sub>2</sub> ( <sub>1</sub> A <sup>1</sup> ) | 5     | 4                | 0.1382           | 0.0065 | 0.1279 | CH <sub>3</sub> Cl            | 6     | 13               | 0.1024           | 0.0165 | 0.0365 |
| CH <sub>3</sub> OH                              | 7     | 9                | 0.1445           | 0.0060 | 0.0268 | CH <sub>3</sub> SH            | 8     | 13               | 0.0947           | 0.0319 | 0.1099 |
| Cl <sub>2</sub>                                 | 9     | 17               | 0.0748           | 0.0196 | 0.0316 | ClF                           | 10    | 13               | 0.1128           | 0.0167 | 0.0249 |
| CO  | 11    | 7                | 0.1528           | 0.0061 | 0.0421 | CO <sub>2</sub>               | 12    | 11               | 0.1461           | 0.0070 | 0.0272 |
| F <sub>2</sub>                                  | 13    | 9                | 0.1766           | 0.0121 | 0.0098 | H <sub>2</sub> CO             | 14    | 8                | 0.1473           | 0.0076 | 0.0279 |
| H <sub>2</sub> O                                | 15    | 5                | 0.1854           | 0.0043 | 0.0115 | H <sub>2</sub> O <sub>2</sub> | 16    | 9                | 0.1478           | 0.0041 | 0.0139 |
| HCl   | 17    | 9                | 0.1283           | 0.0192 | 0.0353 | HCN                           | 18    | 7                | 0.1445           | 0.0066 | 0.0487 |
| HF  | 19    | 5                | 0.2233           | 0.0102 | 0.0055 | He                            | 20    | 1                | 0.3114           | 0.0137 | 0.0276 |
| LiF   | 21    | 6                | 0.1939           | 0.0108 | 0.0567 | LiH                           | 22    | 2                | 0.1579           | 0.0027 | 0.1268 |
| Mg  | 23    | 6                | 0.0652           | 0.0329 | 0.0410 | N <sub>2</sub>                | 24    | 7                | 0.1516           | 0.0024 | 0.0518 |
| Na <sub>2</sub>                                 | 25    | 11               | 0.0213           | 0.0086 | 0.1054 | Na <sup>+</sup>               | 26    | 5                | 0.1226           | 0.0148 | 0.1140 |
| NH <sub>3</sub>                                 | 27    | 5                | 0.1452           | 0.0017 | 0.0422 | NaCl                          | 28    | 14               | 0.1089           | 0.0167 | 0.0848 |
| Ne  | 29    | 5                | 0.2740           | 0.0106 | 0.0265 | SO <sub>2</sub>               | 30    | 16               | 0.1090           | 0.0292 | 0.0960 |
| Be  | 31    | 2                | 0.1989           | 0.0051 | 0.1070 | B <sup>+</sup>                | 32    | 2                | 0.2574           | 0.0049 | 0.1678 |
| CH <sub>4</sub>                                 | 33    | 5                | 0.1627           | 0.0083 | 0.0428 | H <sub>2</sub>                | 34    | 1                | 0.2011           | 0.0001 | 0.0067 |
| Li <sup>+</sup>                                 | 35    | 1                | 0.5497           | 0.0049 | 0.1568 |                               |       |                  |                  |        |        |

**Table 2** Self-adjusting Cartesian grid (SACG) bin attributes and parameters. For a bin attribute  $A$ , the value of  $A$  for a bin  $b$  is denoted as  $b.A$ . Arrays are denoted with square brackets [ ]. See Fig. 1 for construction algorithm diagram

| Attribute                     | Notation    | Description   |
|-------------------------------|-------------|---|
| Value                         | $b.v$       | Value of the potential in the bin                                     |
| Weight                        | $b.w$       | Weight associated with the bin  |
| Count                         | $b.c$       | Number of data points in the bin                                      |
| Side length                   | $b.s$       | Side length of the square bin   |
| Coordinates                   | $(b.x,b.y)$ | Cartesian coordinates on the chosen density variable plane of the bin |
| Data index                    | $b.DI[ ]$   | Array storing indices of data points located in the bin               |
| Parameter                     | Notation    | Description   |
| Default side length           | $S$         | Default side length   |
| Minimum side length tolerance | $S$         | Minimum side length allowed for a bin                                 |
| Maximum count tolerance       | $\bar{C}$   | Maximum number of points allowed to be in a single bin                |
| Data set                      | $D(p)$      | Input data set  |

some form of interpolation in between points to determine a map from  $D(p)$  to the original function.<sup>20</sup> There are no basis functions, and thus no problem of over-fitting, and in the data-set limit, the grid reproduces the true function exactly.†

This is not a practical way forward as simply storing all the data-points is not feasible in the data-set limit. Furthermore, this approach requires too much time to search the stored data for a point when the potential is used in a Kohn–Sham calculation. Instead we propose a histogram map whereby a grid of bins is created, and all data points falling in a bin are averaged to form the value of the bin. If the bins are too large, this scenario clearly represents a poor approximation since the averages cover large portions of the space. The bin size is therefore allowed to vary based on the number of data points in a region: a finer level grid is used in regions where data is abundant, while a coarse level grid is used elsewhere. The resulting histogram will depend heavily on the data set used to train it, but it does preserve the formally nice property of

returning the exact function in the data-set limit, provided that the bin size is allowed to approach zero.

The self-adjusting Cartesian grid (SACG) is an implementation of the above histogram map. The properties of each bin are described in Table 2. For simplicity, the bins are forced to be square. Since the limit of zero bin size ( $s \rightarrow 0$ ) is not achievable due to finite computer precision, in practice the limit  $s \rightarrow S$  is taken.

The construction algorithm is presented in Fig. 1. The default bin side length,  $S$ , the maximum number of points that can lie in a single bin,  $\bar{C}$ , and the data set  $D(p)$  are the input parameters as described in Table 2. The minimum side length tolerance,  $S$ , is set to the precision of the input data set. The first step in construction is initialization of the coarse-level grid. For each data-point, the algorithm either creates a bin on the coarse grid defined by  $S$  using the data point's attributes as initialization parameters, or adds the data point to an existing bin if one exists at the point's coordinates.

Once the initialization is performed, the algorithm executes self-adjustment by first searching the grid for bins to be quartered. Quartering is the process by which a bin divides itself into smaller bins, quartering in the case of two-dimensional bins. A bin,  $b$ , is quartered if  $b.c > \bar{C}$  and  $(b.s/2) \geq S$ . When

† Note that the choice of interpolation was not specified and could, in some cases, suffer from the problems of function-based fitting schemes; namely over-fitting and incompleteness of basis set.

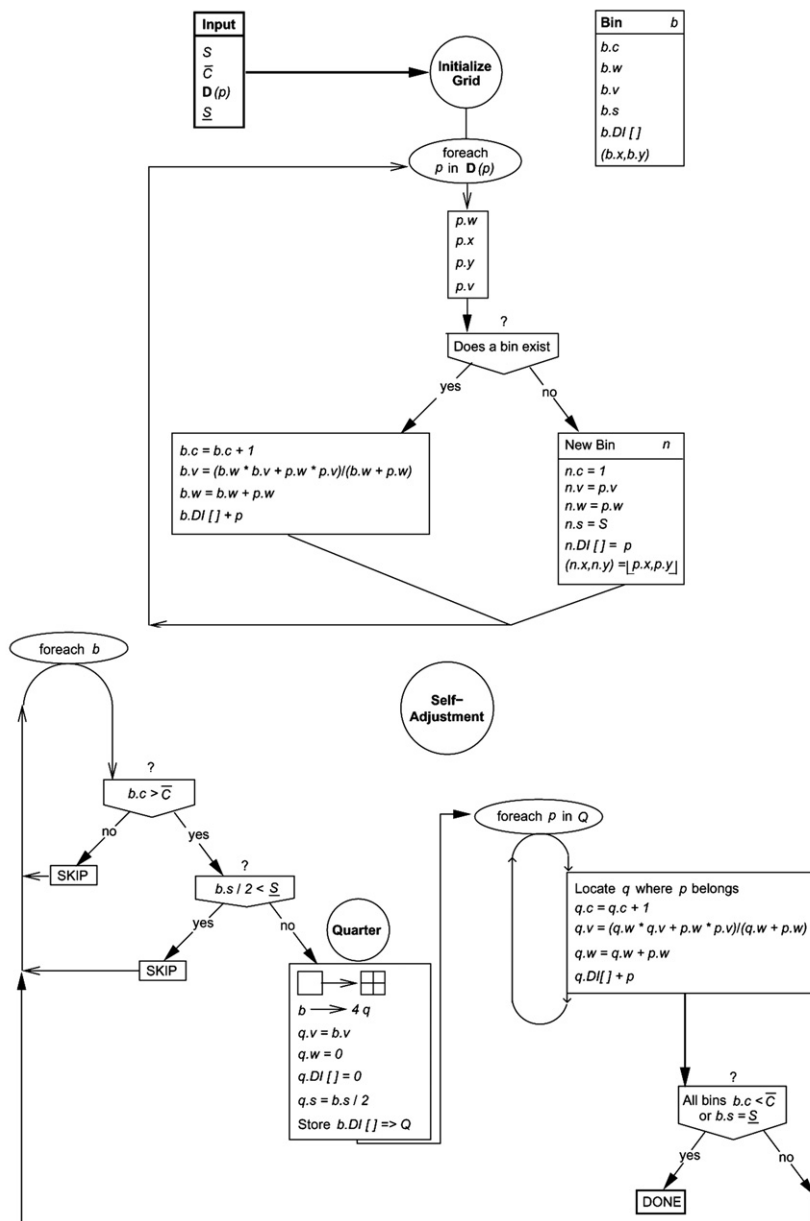


**Fig. 1** Construction algorithm diagram. See Table 2 for explanation of SACG grid attributes and parameters.  $b$  stands for a general bin,  $q$  for a general quarter.

a quartering event occurs, the smaller quarters are initialized to have the value of the original bin, and a side length of  $\frac{1}{2}$  of the original bin. The initial weight is set to 0. The specific data points contained in quartered bins are then placed in the correct quarters. The quarter retains the value of its parent bin if no data point falls in the quarter. This provides an alternative to extrapolation. Since the quarters have weights initialized to zero, the quarter value is overridden if a data point falls in the quarter. The self-adjustment process is carried out until all bins have less than  $\bar{C}$  points, or side lengths equal to  $S$ .

The description presented here is geared toward two-dimensional potentials, but the algorithm is easily generalized to  $N$  dimensions in the obvious way.

The output of the procedure is a numerical table representing the grid. The properties of the potential lookup table are shown in Table 3.

Ultimately, we want to use a SACG map (potential) as an exchange–correlation potential in a Kohn–Sham calculation. During the calculation, the Kohn–Sham equations are solved self-consistently, and the potential is needed at all spatial

points. At each point in space, there are values of  $\rho(\mathbf{r})$ ,  $|\nabla\rho(\mathbf{r})|$ ,  $\nabla^2\rho(\mathbf{r})$ ,  $\nabla\rho(\mathbf{r})\cdot\nabla\nabla\rho(\mathbf{r})\cdot\nabla\rho(\mathbf{r})$ , etc. available, and depending on which density variables were used to construct the map, these can be used to access the SACG potential to return  $v_{xc}^{SACG}$  for that point. The value returned is the value of the bin where the point  $(x,y)$  falls on the grid, for some input  $(x,y)$ . Thus to return a value, all that is needed is an efficient searching algorithm to locate the appropriate bin in the grid. The searching algorithm is shown in Fig. 2.

Once a point is requested, the algorithm first calculates the position of the virtual bin for that point. The virtual bin is the coarse-level bin the point would lie in if it existed. The existence of this virtual bin is then tested. If it does not exist, the return value is governed by the particular method of extrapolation chosen. If the virtual bin does exist, the algorithm searches through all possible  $s$  values to find the smallest bin the point lies in, and returns the value of that bin. Thus the finest level of detail is used that is available.

Several extrapolation procedures were investigated. The proximity extrapolation procedure involves locating the closest

**Table 3** Specific grid properties included in the self-adjusting Cartesian grid (SACG) potential lookup table. See Fig. 2 for search algorithm diagram

| Property          | Notation       | Description   |
|-------------------|----------------|---|
| Side length array | $S[]$          | Sorted list of all side lengths present in the grid |
| Coordinate arrays | $b.x[], b.y[]$ | Arrays storing x and y coordinates of each bin      |
| Value array       | $b.v[]$        | Array storing potential values for each bin         |
| Weight array      | $b.w[]$        | Array storing weights for each bin                  |

filled bin and returning that value for the point. Another routine defines some radius whereby the weighted average of all bins whose centers lie within the radius from the requested  $(x,y)$  point is returned. Both procedures gave similar results, and ultimately the proximity extrapolation was used since it was faster.

The searching algorithm naturally slows down the more intricate the grid. Thus although the SACG has the nice formal property of reducing to the exact function as  $s \rightarrow 0$  in the data-set limit, it is not a practical limit when the potential is used in Kohn–Sham calculations. Note that speed is a major advantage for function based fitting since the cost of evaluating a function computationally is minimal.

The focus of the present investigation is the accuracy of the SACG approach, and the efficiency of the searching procedure is of secondary importance. However, the searching algorithm lends itself to efficient data retrieval algorithms that scale as  $\log_2 kN$ , where  $k$  is the number of dimensions of the SACG potential, and  $N$  is the number of bins.

#### 4 Application to two-dimensional potentials

We must first establish the credibility of the SACG approach as a viable method of constructing a map from density variables of choice to the exchange–correlation potential. The best testing criterion for an SACG potential is how well it performs in Kohn–Sham calculations. As mentioned in the introduction, with  $v_{xc}$  we can solve the Kohn–Sham equations for the Kohn–Sham eigenvalues and orbitals, which give the electron density through eqn. (2). The testing criteria then consist of comparing Kohn–Sham eigenvalues and properties of the density.

Solving the Kohn–Sham equations for specific systems using SACG potentials was implemented in the CADPAC<sup>21</sup> suite of *ab initio* and density functional programs. Evaluation of the

total energy expression requires an explicit form for the exchange–correlation functional  $E_{xc}$ . Since we do not have a  $E_{xc}^{SACG}[\rho]$ , we are forced to use another functional, and the energies obtained in the self-consistent calculations are *not* consistent with the densities from the Kohn–Sham orbitals. However, convergence of the Kohn–Sham calculation is determined by the change in the density matrix within CADPAC, and the densities are consistent with the exchange–correlation potential used. In all calculations with SACG potentials the BLYP<sup>22,23</sup> exchange–correlation functional was used along with a TZ2P basis set.<sup>19</sup>

As discussed in section 3, a two-dimensional SACG map should be able to exactly reproduce a function of just two variables in the data-set limit. Therefore, the SACG methodology was first tested against the analytical approximation to the exchange–correlation potential of van Leeuwen and Baerends (LB94)<sup>5</sup> to test its performance of fitting a function of only  $\rho$  and  $|\nabla\rho|$ . Anticipating fitting the  $v_{xc}^{ZMP}$  data (section 5), we fit the LB94 potential for the same data set. For every  $(\rho, |\nabla\rho)$  pair that occurs in the ZMP data set, we include  $v_{xc}^{LB94}(\rho, |\nabla\rho)$  in the LB94 fit set. We use a weight of one for all data points in the LB94 fit set so the bin values represent non-weighted averages of the points in the bin.

Different combinations for the parameters  $S$  and  $\bar{C}$  in the SACG construction method (section 3) were tried. For the SACG procedure to approach the function it is fitting, ideally  $\bar{C}$  would be set to 1, but there is a tradeoff of accuracy and speed. With the large amount of data in the ZMP fit set (130 330 points),  $\bar{C} = 50$  was found to be sufficient. Investigations showed that greater accuracies were achieved with smaller  $S$  values and more extrapolation, and  $S$  was chosen to be 0.5 in the units of the chosen density variables. In all discussions below, the SACG potentials are denoted as

$$\text{fitSACG}(x,y) \Big|_{\bar{C}}^S \quad (18)$$

where  $(x,y)$  are the density variables used in the map  $(x,y) \rightarrow v_{xc}^{\text{fit}}$ . Table 1 shows the absolute root mean square (RMS) errors in occupied eigenvalues between the LB94 and  $\text{LB94}^{\text{SACG}}(\rho, |\nabla\rho)|_{50}^{0.5}$  potentials where the RMS error is defined as

$$\text{RMS} = \sqrt{\frac{\sum_i^N (O_i - O_i^{\text{true}})^2}{N}} \quad (19)$$

where  $O_i$  is the value of some calculated property,  $O_i^{\text{true}}$  is the true value of the property, and  $N$  is the number of properties included in the error. The majority of the absolute RMS errors are  $10^{-3} E_h$ , which is roughly 1 kcal mol<sup>-1</sup>. It is evident that the  $\text{LB94}^{\text{SACG}}(\rho, |\nabla\rho)|_{50}^{0.5}$  potential is reproducing the eigenvalues of the analytic LB94 potential for the 35 systems comprising the fit set.

We examine differences in the densities directly through the quantity

$$D = \int (\rho(\mathbf{r})_{\text{method}} - \rho(\mathbf{r})_{\text{true}})^2 d\mathbf{r} \quad (20)$$

where in this instance,  $\rho(\mathbf{r})_{\text{true}}$  is the density from the analytic LB94 potential and  $\rho(\mathbf{r})_{\text{method}}$  is the density from

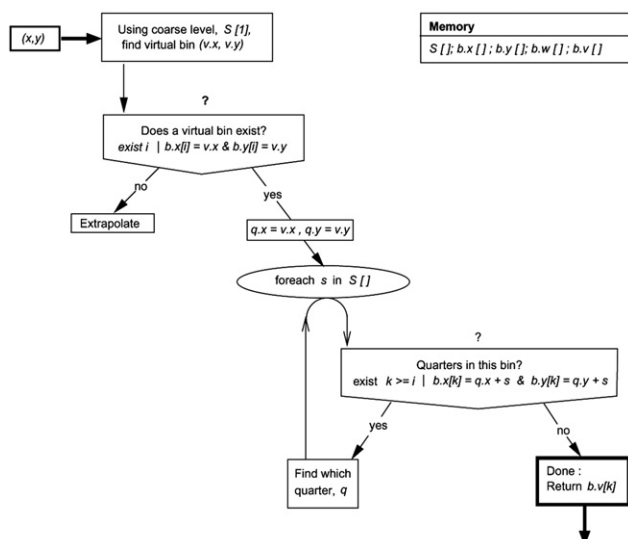


**Fig. 2** Search algorithm diagram. See Table 3 for explanation of SACG grid properties.  $q$  stands for a general quarter.

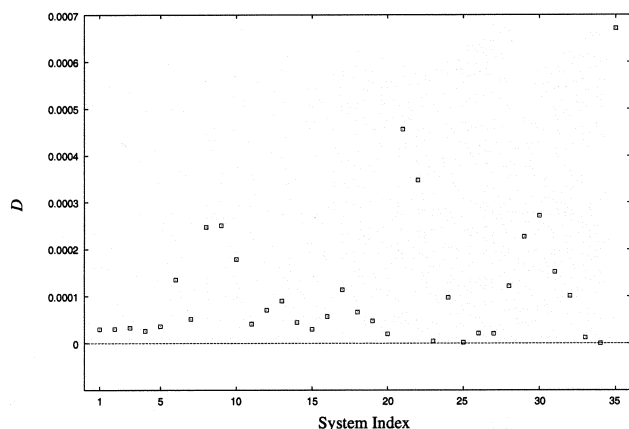


**Fig. 3** Differences between LB94 and  ${}^{\text{LB94}}\text{SACG}(\rho, |\nabla\rho)|_{50}^{0.5}$  densities,  $D$  (eqn. (20)). System indices are listed in Table 1.

${}^{\text{LB94}}\text{SACG}(\rho, |\nabla\rho)|_{50}^{0.5}$ . Plots of this quantity for each system are shown in Fig. 3. These differences are typically  $10^{-4}$  indicating that the densities produced by the two potentials from self-consistent Kohn–Sham calculations are essentially equivalent.

The  ${}^{\text{LB94}}\text{SACG}(\rho, |\nabla\rho)|_{50}^{0.5}$  potential is equivalent to the analytic LB94 potential for the purpose of solving the Kohn–Sham equations. Thus the two-dimensional SACG method is an effective tool for constructing a numerical map from two density variables,  $(x, y)$ , to the exchange–correlation potential,  $v_{\text{xc}}$ , for the case that  $v_{\text{xc}}$  is a function of  $(x, y)$ .

## 5 Application to ZMP data

As demonstrated in the last section, the two-dimensional SACG approach is effective in mapping  $(x, y) \rightarrow f(x, y)$ , for some function  $f(x, y)$ . When applied to  $f = v_{\text{xc}}^{\text{ZMP}}$ ,  $(x, y)$  are not known, but we are motivated by the success of GGA approximations to consider  $(\rho, |\nabla\rho)$  as the variables of the SACG potential. The potential constructed with the ZMP data with the Tozer–Handy (TH) shifts<sup>16</sup> is denoted as  ${}^{\text{ZMP-TH}}\text{SACG}(\rho, |\nabla\rho)|_{50}^{0.5}$ . For every  $(\rho, |\nabla\rho)$  pair that occurs on a grid point in the ZMP data set, we include  $v_{\text{xc}}^{\text{ZMP}} + C_{\text{sys}}^{\text{TH}}$  for that grid point in the ZMP fit set. Note that the factor of  $\frac{1}{2}$  in eqn. (17) is implicit in the TH shifts (Table 1). Initially the weights used were the quadrature weights on the molecular grid from the ZMP calculations. However, investigations show that greater accuracies are achieved with all weights equal to 1. In order to directly compare SACG and ZMP eigenvalues, the  ${}^{\text{ZMP-TH}}\text{SACG}(\rho, |\nabla\rho)|_{50}^{0.5}$  eigenvalues are corrected for the added TH shifts. The absolute RMS errors in the corrected  ${}^{\text{ZMP-TH}}\text{SACG}(\rho, |\nabla\rho)|_{50}^{0.5}$  eigenvalues and the ZMP eigenvalues are shown in Table 1.

The spread in errors is much more apparent than in the test on LB94 data presented above. The majority of the RMS errors are  $10^{-2} E_{\text{h}}$ , but there is a large group of systems with  $10^{-1} E_{\text{h}}$  differences.

The goal of the SACG methodology is to accurately reproduce the potential from which the fitting data set  $D(\rho)$  comes. Thus as applied to the ZMP data set, the SACG potential should be reproducing the ZMP density properties. For density comparisons, the ZMP density should be identical to the input coupled-cluster (CC) density used in the ZMP method if convergence to the limit  $\lambda \rightarrow \infty$  was attained. Thus to measure how close the SACG method is expected to come to reproducing ZMP densities, we compare CC-ZMP differences,  $D_{\text{CC-ZMP}}$  (eqn. 20). For thoroughness,  $D$  quantities for differences with ZMP densities for CC, BLYP, LB94 and  ${}^{\text{ZMP-TH}}\text{SACG}(\rho, |\nabla\rho)|_{50}^{0.5}$  densities are shown in Fig. 4.

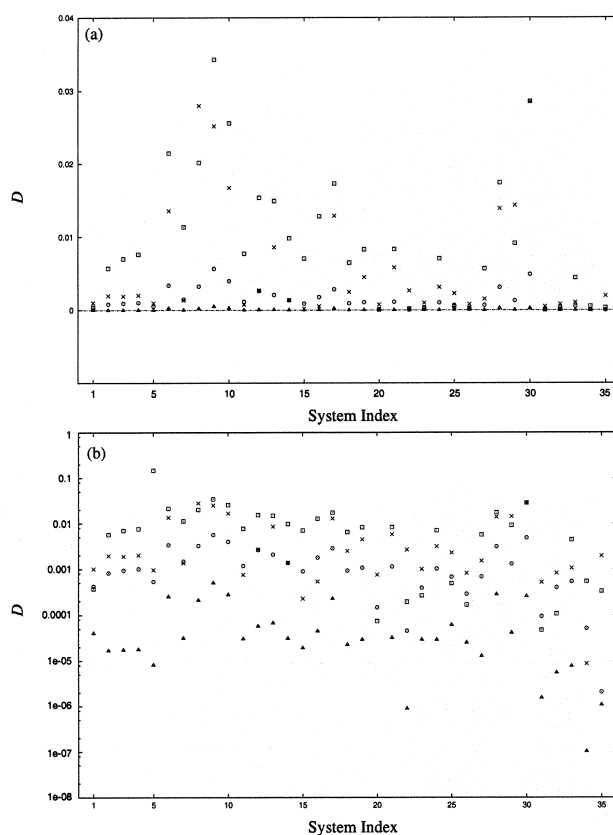


**Fig. 4** Differences between ZMP and  ${}^{\text{ZMP-TH}}\text{SACG}(\rho, |\nabla\rho)|_{50}^{0.5}$  densities,  $D$  (eqn. (20)): true = ZMP,  $\Delta$  method = CC,  $\circ$  method = BLYP,  $\square$  method = LB94,  $\times$  method =  ${}^{\text{ZMP-TH}}\text{SACG}(\rho, |\nabla\rho)|_{50}^{0.5}$ . (a) normal scale, (b) logarithmic scale. System indices are listed in Table 1.

It is interesting to note that BLYP densities are generally closer to the ZMP densities than  ${}^{\text{ZMP-TH}}\text{SACG}(\rho, |\nabla\rho)|_{50}^{0.5}$ . Although  ${}^{\text{ZMP-TH}}\text{SACG}(\rho, |\nabla\rho)|_{50}^{0.5}$  is not the closest to the ZMP density, it is overall closer than the LB94 potential which is expected.

In summary the  ${}^{\text{ZMP-TH}}\text{SACG}(\rho, |\nabla\rho)|_{50}^{0.5}$  potential is only part of the way to the ultimate goal of reproducing ZMP energetics and densities. Examining the construction of the SACG potential, we recognize four reasons for this discrepancy: insufficient fit data, extrapolation errors, errors in the  $C_{\text{sys}}$  values, and the approximation of only including two density variables.

It is evident from the tests against the LB94 potential in section 4 that the data points in the fit set were enough to construct  ${}^{\text{LB94}}\text{SACG}(\rho, |\nabla\rho)|_{50}^{0.5}$ . We therefore eliminate insufficient data as the cause, but do note that we are confining this discussion to representation of the fit set systems, and the broad applicability of a SACG potential requires a broad fit set.

To test the effect of different extrapolation routines, SACG potentials created from data from known potentials were used with proximity and analytical extrapolation, where the form of the analytic potential was used when a point was extrapolated. No differences in results were observed, and we therefore eliminate extrapolation as the cause of the differences.

We must conclude then that the problem lies with either the values of  $C_{\text{sys}}$  used, or with the two-dimensional approximation. Note that a true GGA functional is written as

$$E_{\text{xc}}^{\text{GGA}}[\rho] = \int f(\rho(\mathbf{r}), |\nabla\rho(\mathbf{r})|) d\mathbf{r} \quad (21)$$

Taking the functional derivative using results from the calculus of variations,<sup>1</sup> we find

$$v_{\text{xc}}^{\text{GGA}} = v(\rho(\mathbf{r}), |\nabla\rho(\mathbf{r})|, \nabla^2\rho(\mathbf{r}), \nabla\rho(\mathbf{r}) \cdot \nabla\nabla\rho(\mathbf{r}) \cdot \nabla\rho(\mathbf{r})) \quad (22)$$

Thus a true GGA potential is a function of four density variables. To test the severity of the two-dimensional approximation, we constructed an SACG potential in the  $(\rho, |\nabla\rho|)$  plane using BLYP<sup>22,23</sup> potential data, since  $v_{xc}^{BLYP}$  is a GGA potential. Performing the same comparisons, we found that the RMS errors in the eigenvalues between  $v_{xc}^{BLYP}$  and  $v_{xc}^{SACG(\rho, |\nabla\rho|)_{50}^{0.5}}$  were  $10^{-2} E_h$ , while the  $D$  quantities (eqn. 20) between the two were  $10^{-3}$ . Thus while the two-dimensional approximation limits the capability to reproduce ZMP densities to  $D = 10^{-3}$  (as compared to the  $D_{CC-ZMP}$  values which are  $10^{-5}$  or better), it is not the only factor (Fig. 4), and the shifts must play a role as well.

## 6 Conclusion

In conclusion, we have demonstrated that the self-adjusting Cartesian grid (SACG) histogramming approach is a viable alternative to function based fitting schemes for creating maps from density variables to exchange–correlation potentials. In particular, the SACG scheme does not suffer from the problem of over-fitting, and reproduces the true function in the data-set limit.

The validity of the SACG numerical map was first tested in the case of the analytic LB94 potential,<sup>5</sup> where the exact variables for the map are known from the analytical form. The SACG approach was shown to reproduce LB94 results in Kohn–Sham calculations. The ultimate goal is to create a map from density variables to  $v_{xc}^{ZMP}$ , since  $v_{xc}^{ZMP}$  represents the true exchange–correlation potential for a system. However, the appropriate density variables for the map are not known. A two-dimensional SACG map based on  $(\rho, |\nabla\rho|)$  was found to be not as effective in reproducing  $v_{xc}^{ZMP}$  data. The  $C_{sys}$  values used and the approximation of only two density variables probably caused the discrepancy.

The great advantage of the SACG approach is its flexibility. The addition of more dimensions is a straightforward generalization of the algorithm, the only aspect changing being the details of a quartering event. Within the GGA approximation, as  $\nabla^2\rho$  and  $\nabla\rho\cdot\nabla\nabla\rho\cdot\nabla\rho$  are added as variables, the SACG potential should come closer to being a functional derivative of a GGA functional, which will allow greater accuracies and evaluation of other quantities such as the gradient of the density which is important for determining molecular structures. It could be the case that the GGA-type maps are not the solution to construct  $v_{xc}$ , and further investigation is needed.

The flexibility of the SACG approach allows the investigation of other variables for the map to the exchange–correlation potential. One such variable of interest is the non-local Coulomb potential,  $v_f(\mathbf{r})$ , which arises naturally in the context of ZMP exchange–correlation potentials (eqn. (10)).

We are confident that the principle of constructing the Kohn–Sham exchange–correlation potential from near-exact exchange–correlation potentials of many atoms and molecules is sound. Furthermore, the results presented in this work indicate that this novel approach has promise, and they reveal a clear direction in which to proceed.

## Acknowledgements

JBL would like to thank the Winston Churchill Foundation of the United States for financial support.

## References

- 1 R. G. Parr and W. Yang, *Density-Functional Theory of Atoms and Molecules*, Oxford University Press, Oxford, 1989.
- 2 R. M. Dreizler and E. K. U. Gross, *Density Functional Theory: An Approach to the Quantum Many-Body Problem*, Springer-Verlag, Berlin, 1990.
- 3 W. Kohn and L. J. Sham, *Phys. Rev., Sect. A*, 1965, **140**, 1133.
- 4 P. Hohenberg and W. Kohn, *Phys. Rev., Sect. B*, 1964, **136**, 864.
- 5 R. van Leeuwen and E. J. Baerends, *Phys. Rev. A*, 1994, **49**, 2421.
- 6 M. Levy and J. P. Perdew, *Phys. Rev. A*, 1985, **32**, 2010.
- 7 D. J. Tozer, V. E. Ingamells and N. C. Handy, *J. Chem. Phys.*, 1996, **105**, 9200.
- 8 Q. Zhao, R. C. Morrison and R. G. Parr, *Phys. Rev. A*, 1994, **50**, 2138.
- 9 M. Levy and J. P. Perdew, in *Density Functional Methods in Physics*, ed. R. M. Dreizler and J. da Providencia, Plenum Press, New York, 1985, 11.
- 10 Q. Zhao and R. G. Parr, *J. Chem. Phys.*, 1993, **98**, 543.
- 11 U. Fermi and E. Amaldi, *Mem. R. Accad. Ital., Cl. Sci. Fis. Mat. Nat. Biol.*, 1934, **6**, 117.
- 12 J. P. Perdew, R. G. Parr, M. Levy and J. L. Balduz, Jr., *Phys. Rev. Lett.*, 1982, **49**, 1691.
- 13 J. P. Perdew and M. Levy, *Phys. Rev. Lett.*, 1983, **51**, 1884.
- 14 J. F. Janak, *Phys. Rev. B*, 1978, **18**, 7165.
- 15 J. Katriel and E. R. Davidson, *Proc. Natl. Acad. Sci., USA*, 1980, **77**, 4403.
- 16 D. J. Tozer and N. C. Handy, *J. Chem. Phys.*, 1998, **108**, 2545.
- 17 F. A. Hamprecht, A. J. Cohen, D. J. Tozer and N. C. Handy, *J. Chem. Phys.*, 1998, **109**, 6264–6721.
- 18 R. Kobayashi, N. C. Handy, R. D. Amos, G. W. Trucks, M. J. Frisch and J. A. Pople, *J. Chem. Phys.*, 1991, **95**, 6723.
- 19 T. H. Dunning Jr., *J. Chem. Phys.*, 1971, **55**, 716.
- 20 G. K.-L. Chan and N. C. Handy, *J. Chem. Phys.*, 2000, **112**, 5639.
- 21 R. D. Amos, I. L. Alberts, J. S. Andrews, S. M. Colwell, N. C. Handy, D. Jayatilaka, P. J. Knowles, R. Kobayashi, N. Koga, K. E. Laidig, P. E. Maslen, C. W. Murray, J. E. Rice, J. Sanz, E. D. Simandiras, A. J. Stone, M.-D. Su, D. J. Tozer, *CADPAC 6.5: Cambridge Analytical Derivatives Package: A suite of quantum chemistry programs*, Cambridge, UK, 1998.
- 22 A. D. Becke, *Phys. Rev. A*, 1988, **38**, 3098.
- 23 C. Lee, W. Yang and R. G. Parr, *Phys. Rev. B*, 1988, **37**, 785.